ELSEVIER

Catalysis Today 72 (2002) 63–78

CATALYSIS TODAY

www.elsevier.com/locate/cattod

Supported gold nanoparticles: in-depth catalyst characterization and application in hydrogenation and oxidation reactions

Sabine Schimpf [a], Martin Lucas [a], Christian Mohr [a], Uwe Rodemerck [b], Angelika Brückner [b], Jörg Radnik [b], Herbert Hofmeister [c], Peter Claus [a,*]

[a] *Department of Chemistry, Institute of Chemical Technology II, Technical University of Darmstadt, Petersenstr. 20, D-64287 Darmstadt, Germany*

[b] *Institute for Applied Chemistry, Department of Catalysis, Berlin, Germany*

[c] *Max-Planck Institute of Microstructure Physics, Halle, Germany*

Abstract

Silica, titania, zirconia and alumina supported gold particles of 1–6 nm size, prepared by various synthetic routes (sol–gel technique, deposition–precipitation, metal organic-chemical vapor deposition, impregnation, dip-coating) were employed in the selective hydrogenation of acrolein, crotonaldehyde and 1,3-butadiene and in the low-temperature oxidation of carbon monoxide. In-depth characterization of their structural and electronic properties by transmission electron microscopy (TEM), electron paramagnetic resonance (EPR) and X-ray photoelectron spectroscopy (XPS) was aimed at disclosing the nature of the active sites controlling the hydrogenation and oxidation reactions. The structural characteristics such as mean particle size, size distribution and dispersion depend both on the synthetic method employed and the nature of the support. For extremely small gold particles on titania and zirconia (1.1 and 1.4 nm mean size), conduction electron spin resonance of the metal and paramagnetic F-centers (trapped electrons in oxygen vacancies) of the support were observed. The marked structure-sensitivity observed for hydrogenation properties with decreasing particle size may be attributed to structural and electronic properties due to the quantum-size effect of sufficiently small gold particles. Furthermore, the adaptability of gold particles in coatings is demonstrated for a microchannel reactor.

Keywords: Selective hydrogenation; Supported gold nanoparticles; Carbon monoxide oxidation

1. Introduction

In the last few years, there has been a growing interest in "nanosized" structures in the range of 1–20 nm in many different fields of research, and this has included that of heterogeneous catalysis. Nanoparticles of Pd, Ru, Ni or Pt are used for hydrogenations [1], since on these metals dissociatively adsorbed hydrogen is easily accessible. For a long time only very limited attention was paid to studying catalysis by gold because of its completely filled d-band, accompanied by very low activities [2]. The situation has changed since Haruta [3] reported that CO oxidation could be achieved at room temperature if very small gold nanoparticles were used on suitable supports. The focus on oxidation reactions masked the capabilities of gold in hydrogenation reactions, even though there are promising first examples of possible applications [2]. For instance, in the hydrogenation of α,β-unsaturated aldehydes to give allylic alcohols, the control of intramolecular selectivity is more important than maximum activities. These reactions are an important step

* Corresponding author. Tel.: +49-6151-16-5369; fax: +49-6151-16-4788.
E-mail address: claus@ct.chemie.tu-darmstadt.de (P. Claus).

0920-5861/02/$ – see front matter
PII: S0920-5861(01)00479-5

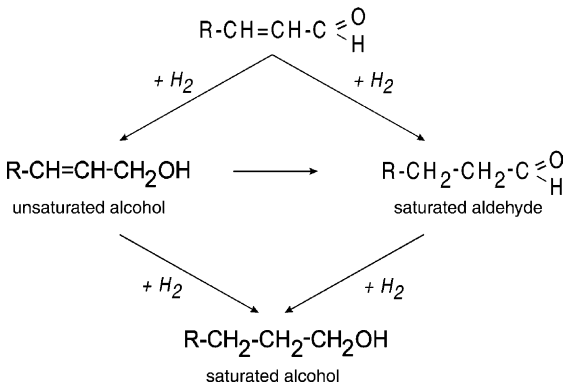

Fig. 1. General scheme for the hydrogenation of α,β-unsaturated aldehydes as acrolein (R: H) or crotonaldehyde (R: CH_3).

in the industrial synthesis of fine chemicals, particularly of pharmaceuticals and cosmetics [4,5] and have therefore attracted much interest for fundamental research in catalysis. A simplified reaction scheme is given in Fig. 1. Because of the stronger negative free reaction enthalpy, thermodynamics favors the hydrogenation of the C=C over the C=O group. Furthermore, the olefinic double bond is more reactive than the C=O group. In addition to the reactions shown in Fig. 1, further reactions such as decarbonylation of aldehydes, dehydration of alcohols and di/oligomerization of unsaturated aldehydes are possible. Hence conventional hydrogenation catalysts mainly provide the saturated aldehyde, but catalysts are necessary to control the intramolecular selectivity. Steric and electronic effects and the structure and morphology of metal particle surfaces are some of the most effective factors controlling intramolecular selectivity [6,7]. Convenient catalysts were developed for the liquid phase hydrogenation of higher α,β-unsaturated aldehydes, e.g. cinnamaldehyde (selectivity >96%) over Pt/Y zeolite [8] and citral (selectivity = 96% at complete conversion) over a $Rh[Sn(n\text{-}C_4H_9)_2]SiO_2$ catalyst [9]. More intriguing feedstocks are the C_3 and C_4 unsaturated aldehydes such as acrolein and crotonaldehyde. Acrolein is considered as the α,β-unsaturated aldehyde most difficult to hydrogenate to allyl alcohol because of the lack of space-filling substituents at the C=C group [6,7,10–13].

In spite of being used almost exclusively in oxidation reactions, we have found recently excellent catalytic properties of supported Ag nanoparticles in the hydrogenation of α,β-unsaturated aldehydes [6,10,14,15]. In the gas phase hydrogenation of acrolein at 453 K and 2 MPa, we achieved a selectivity to allyl alcohol of 50% (conversion = 56%) on an Ag/SiO_2 catalyst [16]. This encouraged us to explore the potential of gold for this reaction. Downsizing the particle size of Au however also affects its electronic character. For Au nanoparticles grown by vapor deposition in ultrahigh vacuum on single crystalline $TiO_2(1\,1\,0)$ surfaces, scanning tunneling spectroscopy revealed a band gap for particles smaller than 4 nm that increases in width with further size reduction giving rise to nonmetallic character [17]. According to these results, significant changes of catalytic properties should be observed with gold particle sizes below 2–3 nm, if the gold mediated hydrogenation depends on metallic character [18].

In these studies, titania and zirconia supported gold particles were employed in the selective hydrogenation of acrolein, whereas silica supported gold particles were used for crotonaldehyde hydrogenation and for low-temperature CO oxidation. To explore the potential of coatings of supported Au particles for catalysis, $Au/MeO_x/Al$ catalyst wafers (MeO_x: Al_2O_3, SiO_2, ZrO_2, TiO_2) were prepared and tested in a microchannel reactor for the selective hydrogenation of 1,3-butadiene. Characterization of the structural and electronic properties of all the catalysts by transmission electron microscopy (TEM), electron paramagnetic resonance (EPR) and X-ray photoelectron spectroscopy (XPS) was aimed at defining the nature of the active sites controlling hydrogenation and oxidation reactions.

2. Experimental

2.1. Preparation of catalysts

Titania, zirconia, silica and alumina supported gold particles 1–6 nm in diameter were prepared by various synthetic routes: deposition–precipitation (DP), impregnation (I), sol–gel technique (SG), coprecipitation (F), incipient wetness (IW), metal organic-chemical vapor deposition (MO-CVD) and dip-coating. An overview of the catalysts prepared and the precursors used is given in Table 1. Three titania-based

Table 1
Preparation techniques and gold and support precursors

Catalyst	Preparation technique	Gold precursor	Support precursor
Au/TiO_2-DP	Deposition–precipitation	$HAuCl_4$	P25 (Degussa)
Au/TiO_2-I	Impregnation	$AuCl_3$	P25 (Degussa)
Au/TiO_2-SG	Sol–gel technique	Gold acetate	TBOT
Au/ZrO_2-F	Coprecipitation	$HAuCl_4$	$ZrOCl_2{\cdot}8H_2O$
Au/ZrO_2-DP	Deposition–Precipitation[a]	$HAuCl_4$	$ZrOCl_2{\cdot}8H_2O$
Au/SiO_2-IW	Incipient wetness	$AuCl_3$	Silica gel, large pore (Alfa)
Au/SiO_2-CVD	Metal organic-chemical vapor deposition	$Me_2Au(acac)$[b]	Silica gel, large pore (Alfa)
Au/Al_2O_3/Al	Dip-coating	$HAuCl_4$	Al_2O_3/Al (spin-coating)

[a] Zirconia was formed in an additional step.
[b] Dimethylgold(III)β-diketone.

catalysts were prepared by the DP, I and SG methods. The support used for the DP and I methods was Degussa P25 titania. The gold precursors for the DP and I methods were $HAuCl_4$ (STREM) and $AuCl_3$ (Aldrich), respectively. In the case of the impregnated catalyst, Au/TiO_2-I, the gold precursor solution consisted of $AuCl_3$ dissolved in distilled water and was added dropwise to the titania. Details of preparation are given in reference [19]. Both catalysts, Au/TiO_2-I and Au/TiO_2-DP were dried (373 K, 12 h), calcined in flowing air (573 K) for 8 h and reduced in flowing hydrogen at 573 K for 3 h. The sol–gel derived titania supported gold catalyst, Au/TiO_2-SG, was prepared by using tetrabutoxytitanium(IV) (TBOT, purchased from Aldrich), gold acetate (99.9% pure, from Alfa), methanol (HPLC grade) and distilled water as described earlier [19]. A zirconia supported gold catalyst, noted as Au/ZrO_2-F, was prepared by coprecipitation using aqueous solutions of $HAuCl_4$ and $ZrOCl_2{\cdot}8H_2O$. This catalyst was dried at 393 K for 8 h and calcined and reduced as the catalysts mentioned above. While for this catalyst the support was formed from zirconyl nitrate simultaneously with precipitation of gold hydroxide, in the case of the Au/ZrO_2-DP catalyst the zirconia was preformed in an additional step [20]. The Au/SiO_2-IW catalyst was prepared by the IW method using an aqueous solution of gold chloride (Aldrich) and silica (silica gel large pore, Alfa) as support. This catalyst was also dried at 393 K for 8 h and calcined and reduced as for the catalysts mentioned above. A Au/SiO_2-CVD catalyst was prepared according to the preparation method described by Haruta and coworkers [21]; silica gel large pore, Alfa, was used as support. The coating of the microchannels with alumina, silica, zirconia and titania was achieved by spin-coating, alumina also by dip-coating. In the latter case coating of the microchannels was achieved by the deposition of a pseudobohemite primer prepared by dispersing a commercial aluminum hydroxide powder (Disperal®, Sasol) in HNO_3 aqueous solution. The microstructures were then dipped into the dispersion and dried at room temperature followed by dip-coating with an aqueous solution of the gold precursor ($HAuCl_4$ or $AuCl_3$), drying at 393 K in flowing air and at 573 K in flowing Ar and reduction at 573 K in flowing hydrogen.

2.2. Characterization

Atomic Emission Spectroscopy. The gold contents of the catalysts were determined by atomic emission spectroscopy with inductively coupled plasma (AES-ICP, Perkin Elmer Optima 3000XL) after dissolving the materials in a mixture of HF/HNO_3 using an MDS-2000 microwave unit (CEM). The designations of the supported gold catalysts used in this study and their metal contents are given in Table 2.

TEM, high resolution electron microscopy (*HREM*). Qualitative and quantitative characterization of the catalysts were carried out using a JEM 100C operating at 100 kV for TEM in bright and dark field modes. Crystallinity and crystal structure of the samples were evaluated from selected area electron diffraction (SAED) patterns as well as by HREM done at a JEM 4000EX operating at 400 kV. For TEM examination the catalysts were dissolved in isopropanol, dispersed carefully in an ultrasonic bath and then deposited

Table 2
Gold content, surface area, pore volume, Au particle sizes and degree of dispersion estimated by TEM analysis

Catalyst	Au content (wt.%)	Surface area (m^2/g)	Pore volume (ml/g)	$\bar{d}_{Au}$ (nm)[a]	msd (nm)[b]	D_{Au}[c]
Au/TiO_2-DP	1.7	42	0.35	5.3	0.3	0.36
Au/TiO_2-I	2.9	42	0.38	2.0	0.4	0.47
Au/TiO_2-SG	4.8	117	0.17	1.1	0.2	0.78
Au/ZrO_2-F	1.0	151	0.37	1.4	0.3	0.63
Au/ZrO_2-DP	1.2	127	0.10	3.8[d]	2.9	0.36
Au/SiO_2-IW	1.6	171	0.85	3.9	2.3	0.16
Au/SiO_2-CVD	2.4	NE[e]	NE	1.4	0.3	0.70
Au/Al_2O_3/Al	0.02[f]	NE	NE	NE	NE	NE

[a] Mean diameter of log-normal distribution.
[b] Mean square displacement.
[c] Estimated from the ratio of the number of surface atoms to the total number of atoms as calculated for the mean particle size by assuming closed shell particles of spherical shape.
[d] Bimodal particle size distribution (2.1 and 7.4 nm) [20].
[e] Not estimated.
[f] Estimated by peeling off the coating (392.56 mg) of two wafers.

on carbon-coated copper grids. Image processing for contrast enhancement and image evaluation was done at digitized electron micrographs by means of the programs Digital Micrograph (Gatan) and NIH Image [22].

EPR. EPR spectra of samples Au/TiO_2-SG, Au/TiO_2-DP, Au/TiO_2-I, Au/ZrO_2-F and TiO_2 were recorded with the cw-spectrometer ELEXSYS 500-10/12 (Bruker) in X-band ($\nu = 9.515$ GHz) at 77 and 293 K using a finger dewar. The magnetic field was measured with reference to a standard of 2,2-diphenyl-1-picrylhydrazyl hydrate (DPPH). Reduction of the catalysts was performed in flowing hydrogen (45 ml/min) at 723 K (samples Au/TiO_2-SG and TiO_2) and 573 K (sample Au/ZrO_2), respectively, with an EPR flow cell consisting of two coaxial tubes similar to that described by Mesaros and Dybowski [23] EPR spectra were recorded after treatment in H_2 without contact to ambient atmosphere.

2.3. Selective hydrogenation and oxidation reactions

Selective hydrogenation of acrolein and crotonaldehyde. Gas phase hydrogenation of acrolein (Ac, purchased from Aldrich) was carried out in a computer-controlled fixed-bed microreactor system which allows the performance of high-pressure gas phase hydrogenations (2 MPa) and which has been described in detail elsewhere [24]. The reactor effluents were analyzed on-line using an HP 5890 gas chromatograph, equipped with a flame ionization detector and a 30 m J&W DB-WAX capillary column. The gold catalysts were reduced in situ under the conditions described above. The reaction conditions of the acrolein hydrogenation were: temperature range $453\,K \leq T \leq 593\,K$, total pressure $p = 2$ MPa, molar ratio $H_2/Ac = 20$, reciprocal space time $W/F^0_{Ac} = 15.3\,g_{cat}\,h\,mol^{-1}$ where W is the weight of the catalyst (0.23 g, particle size 0.2–0.5 mm) and F the molar flow of acrolein. Temperatures in the range 513–553 K were required for zirconia supported gold catalysts to be active, and conversion data up to 10% were obtained. Using Au/TiO_2 catalysts, acrolein hydrogenation to allyl alcohol and propanal started at lower temperatures around 473 K. For the purpose of comparison, the catalytic data are reported at 513 K. All the gold catalysts exhibited good activity maintenance during time on stream (catalytic runs over 3 h). Minimal activity loss was only observed during the first 10 min in the case of Au/TiO_2 catalysts. This could be due to the formation of acrylic acid and formyldihydropyran which were detected as by-products. Note that all the given catalytic data (specific activities, selectivities) are based on steady-state behavior of the catalysts. The selectivities of reaction products were calculated from moles of product formed per moles of acrolein converted and the catalyst activities were expressed as specific activities (on a gram of gold basis).

2.4. Selective hydrogenation of butadiene

Gas phase hydrogenation of butadiene was carried out in the same computer-controlled reactor system using the same analysis system (on-line GC), but with a microchannel reactor instead of the fixed-bed reactor at ambient pressure. The gold catalysts were reduced in situ under the conditions described above. The reaction conditions were: temperature range $493\,K \leq T \leq 553\,K$, total pressure $p = 0.1\,MPa$, molar ratio H_2/butadiene = 10.

2.5. Low-temperature oxidation of carbon monoxide

The gold catalysts were calcined in situ at 773 K. The reaction was performed in a fixed-bed reactor system. For product analysis a mass spectrometer was used. The reaction conditions were: temperature range $257\,K \leq T \leq 303\,K$, total pressure $p = 0.1\,MPa$, $m_{cat} = 100\,mg$, overall gas velocity = 33 ml/min (0.96% CO and 20% oxygen in inert gas).

3. Results and discussion

3.1. Characterization

In Table 2 structural characteristics such as gold content, BET surface area, pore volume and the mean gold particle diameters of the catalysts are summarized. To estimate particle size characteristics, all catalysts were reduced in flowing hydrogen. Highly dispersed, nanometer-sized gold particles in the range 1–6 nm with mostly narrow size distributions have been produced. An approximate degree of gold dispersion was estimated from the ratio of the number of surface atoms to the total number of atoms calculated from the mean particle size by assuming closed shell particles of nearly spherical shape [25]. Comparing the titania supported catalysts, an increase of mean particle size following the sequence SG, I and DP methods is found. In Au/TiO_2-SG extremely small, nearly spherical particles with very narrow size distribution and small mean particle size were observed (Fig. 2). Using the SG method, the characterization is more difficult since the Au particles are embedded in the TiO_2 network. However, by using this method nanoparticles down to 1 nm were achieved without using the stabilizers commonly used in the preparation techniques for Au nanoparticles [26–30]. Au/TiO_2-I exhibits a broader size distribution (Fig. 3). HREM revealed mostly single crystalline small particles and some defect structures for the larger ones. The particles of Au/TiO_2-DP (Fig. 4) are the largest among the titania supported ones. The DP method usually produces mean particle sizes smaller than 5 nm at above pH 6 [31]. The catalyst Au/ZrO_2-DP (Fig. 5) showed a bimodal size distribution and the mean particle size of Au/ZrO_2-F is similar to the size

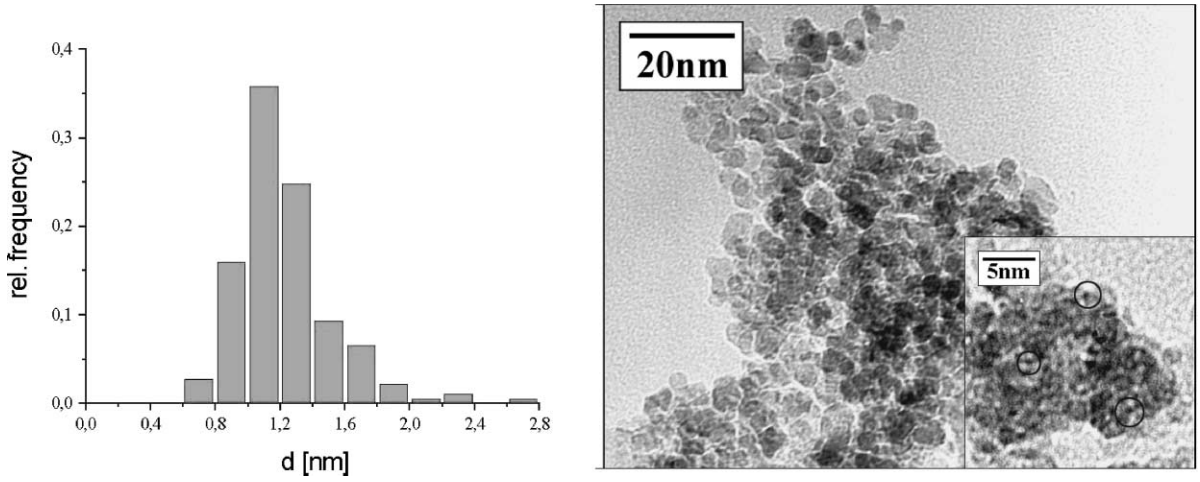

Fig. 2. Size distribution (left) and CTEM overview (right) of the catalyst Au/TiO_2-SG [19].

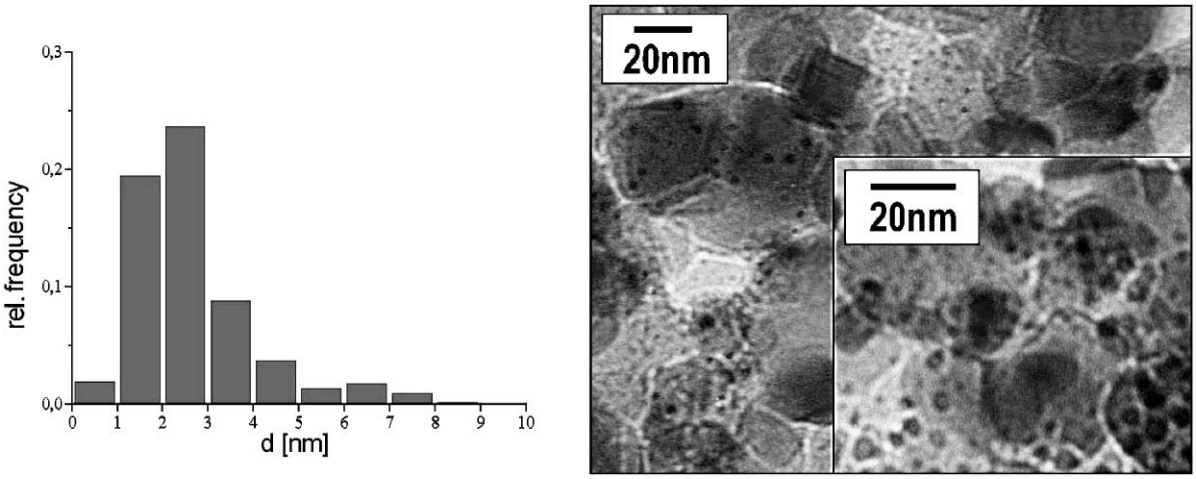

Fig. 3. Size distribution (left) and CTEM overview (right) of the catalyst Au/TiO_2-I [19].

of the sol–gel derived catalyst. These gold particles are in good approximation spherically with a larger amount of lattice defects. Particles smaller than 1 nm, being 'invisible' for TEM, may be present in all the samples. A more detailed description of the TEM investigations is given in [19]. The results show that besides depending on synthesis, the size and morphology of Au nanoparticles are definitely governed by the choice of a suitable oxide support.

The EPR spectrum of the Au/TiO_2-SG sample recorded before reduction in flowing hydrogen (Fig. 6) contains a hyperfine quartet ($A = 4.5$ mT) which may be due to the $g_\perp$-part of Au^{2+} ions (^{197}Au:I = 3:2, 100% natural abundance). This is in agreement with the data measured for Au^{2+} ions in gold fluoride [32]. The quartet is superimposed on a narrow singlet close to the free electron g-value. Upon reduction in H_2 at 723 K the hyperfine quartet vanishes since Au^{2+} ions are reduced to elementary gold (Fig. 6b). Simultaneously, a strong signal at $g = 1.936$ assigned to Ti^{3+} [33] appears which indicates a marked reduction of the support. When the reduced sample is stored in an ambient atmosphere, the Ti^{3+} signal vanishes again with time due to reoxidation, but the narrow singlet

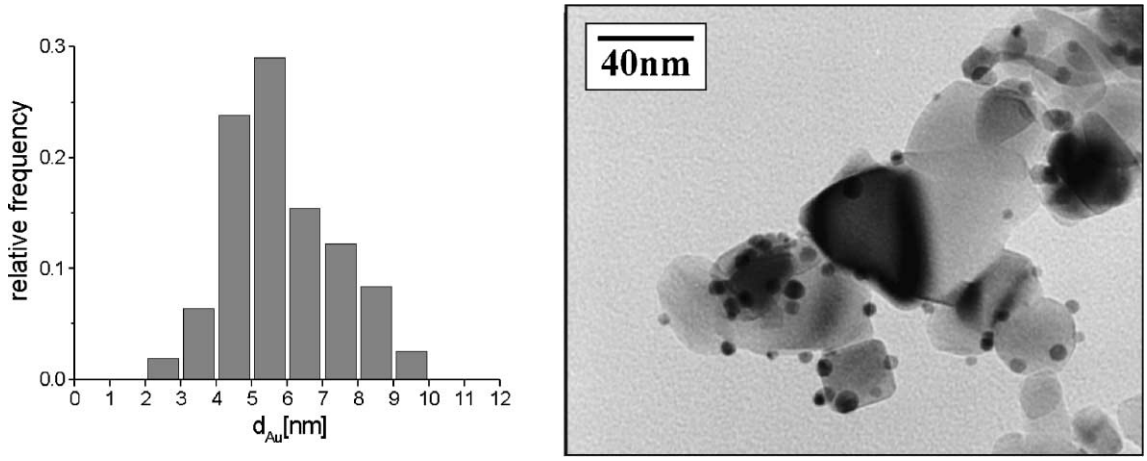

Fig. 4. Size distribution (left) and CTEM overview (right) of the catalyst Au/TiO_2-DP [19].

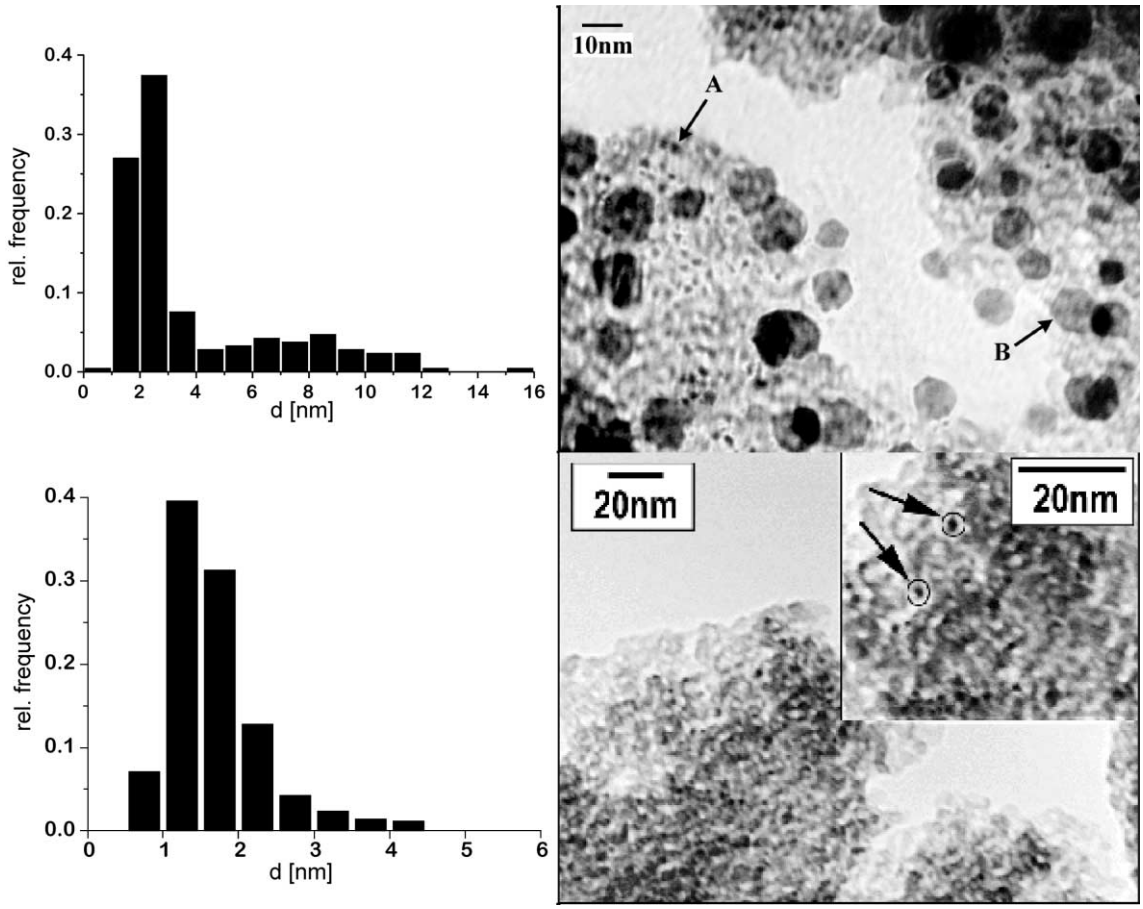

Fig. 5. Size distribution (left) and CTEM overview (right) of the catalysts Au/ZrO_2-DP (upper row) and Au/ZrO_2-F (lower row). Arrows indicate fractions of smaller (A) and larger (B) particles [37].

at $g = 2.0053$ is still present (Fig. 6c and d). While the latter is also detectable at room temperature, the Ti^{3+} signal can only be seen at 77 K due to the short relaxation time. In the case of samples Au/TiO_2-I and Au/TiO_2-DP (not shown here) no signal is visible in the room temperature spectra. The only EPR signal detectable in the spectra of these samples is that of Ti^{3+} at 77 K after reduction. It can be excluded that the singlet at $g = 2.0053$ in Fig. 6a–d is due to CESR of small Au particles as assigned by Monot et al. [34]. This signal is traced to the existence of paramagnetic defects, namely F-centers, i.e. electrons trapped in an oxygen vacancy, within the support after reduction in hydrogen [19]. This was confirmed by the measurements of a sol–gel derived TiO_2 support prepared by the same procedure but without the addition of gold, and the fact that the TiO_2 sample is black after reduction. It is well known that F-centres in ionic crystals give rise to deep colors. For example, ZrO_2 nanopowder with a high concentration of F-centres was found to be brown [35]. During exposure to air the color of reduced TiO_2 turns to white again, the defect signal at 293 K decreases markedly and the characteristic signal for O_2^--radicals appears at 77 K (not shown), the formation of which can be explained by reaction of molecular oxygen with the F-centres. By comparing the EPR results of Au/TiO_2-SG and pure TiO_2 it is quite evident that the singlet at $g' = 2.0053$ in the former is due to the F-centres formed by reduction of the TiO_2 support and does not originate from

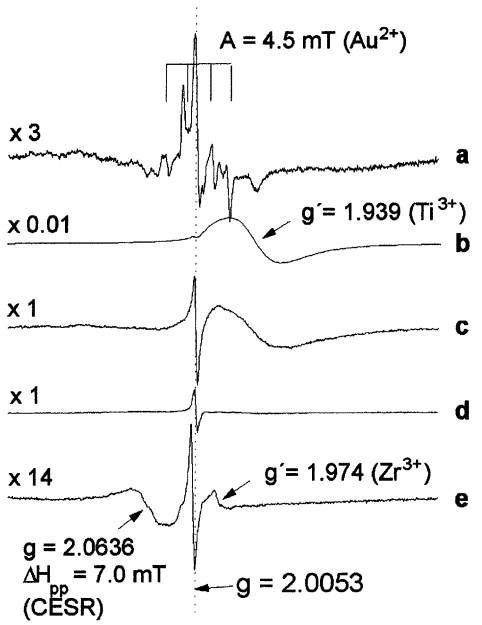

Fig. 6. EPR spectra at 77 K (300 mT < B_0 < 390 mT) of Au/TiO_2-SG after drying at 453 K (a), after reduction at 723 K in H_2-flow (b), after 18 h exposure to ambient atmosphere (c), after exposure to air for several weeks (d), and of Au/ZrO_2-F after reduction at 573 K in H_2-flow and exposure to ambient atmosphere for several weeks (e) [19].

CESR of small Au particles. The EPR spectrum of Au/ZrO_2-F contains a similar narrow singlet near the free electron *g*-value (Fig. 6e) although its intensity is markedly lower than in Au/TiO_2-SG. It is assigned to F-centres in ZrO_2 [35]. Additionally, signals at $g' = 1.974$ for Zr^{3+} and at $g' = 2.0636$ occur. The latter vanishes almost completely after repeated treatment in flowing H_2 at 673 K for 3 h (not shown), while the signal due to the reaction between molecular oxygen and F-centres was also observed after reduction of TiO_2. As with TiO_2, exposure to air leads to the concentration of F-centres decreasing while the line at $g' = 2.0636$ reappears. The large *g*-shift suggests an assignment of this signal to CESR of small Au particles. More details on the EPR measurements on these catalysts are given in [19].

From TEM analysis the nature of the gold particles is clearly visible. With EPR we could find evidence for F-centers, i.e. electrons trapped in an oxygen vacancy, within the support after reduction in hydrogen [19]. Furthermore, XPS of the in situ reduced catalysts revealed a pronounced decrease of the binding energy of Au compared to that of bulk gold [28]. For example, the binding energy of Au $4f_{7/2}$ state shifted to a value of 83.3 eV (Au/TiO_2-SG) compared to the gold bulk value of 84.2 eV (Fig. 7). Further studies are necessary to understand the origin of these experimental findings; they probably result from electron transfer from the partially reduced support to nanosized gold particles. However, the interpretation of these results is under discussion [36] and the preliminary results obtained by Mössbauer spectroscopy did not reveal the presence of negatively charged Au particles.

3.2. Hydrogenation of crotonaldehyde and acrolein

As mentioned in the introduction we started to investigate Au catalysts after successful use of monometallic Ag catalysts. Our first Au catalyst (Au/SiO_2-IW) was examined in the gas phase hydrogenation of crotonaldehyde. The size distribution of gold particles determined by TEM gave a mean diameter of 3.9 nm. Fig. 8 gives the results of the hydrogenation of crotonaldehyde at 533 K and 2 MPa. At a steady-state conversion of about 8% the selectivity to crotyl alcohol was 40% which is considerably higher than when using conventional Group VIII metal hydrogenation catalysts, demonstrating the intrinsic hydrogenation selectivity capability of nanosized gold particles [37]. In contrast, no crotyl alcohol was detected by Bailie and Hutchings [38] during crotonaldehyde hydrogenation if Au was supported on silica. Bailie and Hutchings found that the saturated aldehyde was the main product (selectivity >97%, at 523 K) and the conversion increased from 11 to 22% during time on stream of 180 min. Improved crotyl alcohol selectivities were achieved with Au/ZnO (52% at 9% conversion) and Au/ZrO_2 (38% at 12% conversion) at 527 K (Au loading: 5 wt.%). By comparison with Au/ZnO and Au/ZrO_2, these authors concluded that interfacial sites responsible for C=O group adsorption were absent in the case of SiO_2 and the adjacent large Au particles. Nevertheless, they reported that the crotyl alcohol selectivity further increased by addition of a sulfur-containing compound up to 82% on Au/ZnO. The hydrogenation of crotonaldehyde was also examined by Shibata et al. [39] on ZrO_2-based gold catalysts. While a

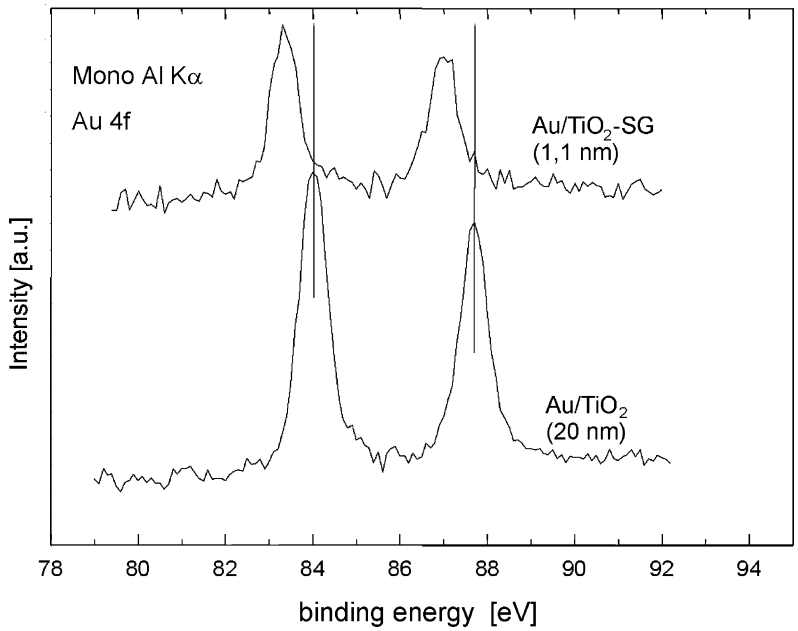

Fig. 7. XPS spectra of Au/TiO_2-SG after reduction at 723 K in H_2-flow and of Au/TiO_2 after reduction at 723 K in H_2-flow [37].

system based on an amorphous alloy was reported to work quite well (with crotyl alcohol selectivities of almost 60% at 10% conversion at 393 K and Au loading of 2 wt.%), an impregnated catalyst had much lower activity and selectivity towards C=O hydrogenation.

After these first results we started to investigate the even more challenging hydrogenation of acrolein

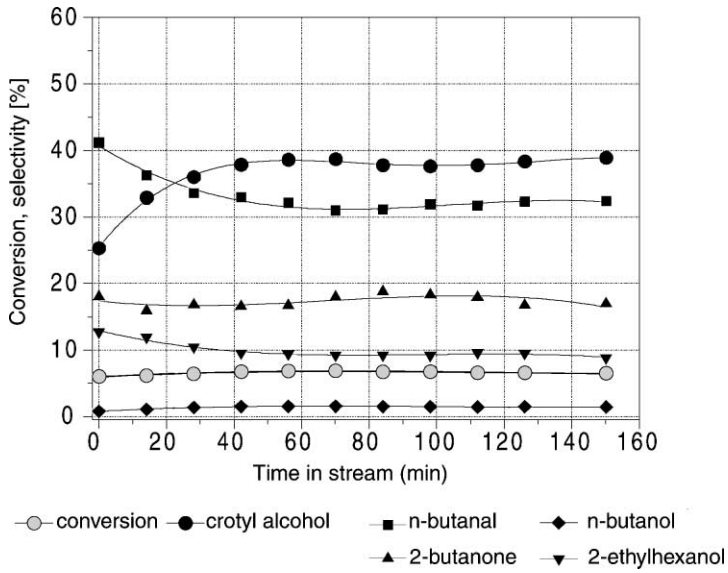

Fig. 8. Hydrogenation of crotonaldehyde over Au/SiO_2-IW ($T = 533$ K), $p_{total} = 2$ MPa, $H_2/CA = 20$, $W/F^0_{Ac} = 19\,g\,h\,mol^{-1}$ [37].

using gold catalysts. The hydrogenation of acrolein over the titania supported catalysts (Au/TiO_2-DP and Au/TiO_2-I) at 453 K and 2 MPa gave allyl alcohol with nearly the same selectivity of 41 and 43%, respectively, at acrolein conversion <10% [19]. It should be noted that this steady-state level of selectivity is up to one order of magnitude higher than in the case of supported Group 8–10 metals used for the hydrogenation of acrolein [11–13,40]. The competitive hydrogenation of the C=C bond of acrolein to propanal mainly accounts for the difference to 100% selectivity, whereas the formation of further possible reaction products (propanol, hydrocarbons, acrylic acid by oxygen transfer from the support and formyldihydropyran) contributes only to a much smaller extent to the product composition. Moreover, considering the size of the gold particles in both catalysts, Au/TiO_2-DP ($d_{Au} = 5.3$ nm) and Au/TiO_2-I ($d_{Au} = 2.0$ m), the selectivity is nearly independent of the particle size. Thus, the hydrogenation of acrolein over Au/TiO_2 catalysts appears to be structure-insensitive for sizes above 2 nm. However, it has to kept in mind that a particular catalytic system can exhibit structure-sensitivity in only a small range of particle sizes [1,41,42]. It is noteworthy that at 453 K the Au/TiO_2-SG and Au/ZrO_2-F catalysts showed no activity, and higher temperatures (513–593 K) had to be applied. Table 3 shows the catalytic properties in terms of activity, apparent activation energy and selectivity data of all catalysts at 513 K [19]. For Au/TiO_2-SG and Au/ZrO_2-F selectivities to the reaction products were independent of acrolein conversion within the whole temperature range, whereas with the catalysts Au/TiO_2-DP and Au/TiO_2-I the selectivity to allyl alcohol was lower due to secondary reactions (formation of propanol and hydrocarbons). However, again the selectivity (about 25%), catalyst activity and also the apparent activation energy did not depend on the gold particle size. Interestingly, with further lowering the gold particle size to 1.4 nm (Au/ZrO_2-F) and 1.1 nm (Au/TiO_2-SG) a drastic decrease in the catalytic activity was observed by up to two orders of magnitude. Likewise the apparent activation energy and the selectivity to allyl alcohol were diminished: the lowest apparent activation energy was found for the Au/ZrO_2-F catalyst with Au particles of 1.4 nm. The findings are in line with the antipathetic structure-sensitivity for a zirconia supported gold catalyst (Au/ZrO_2-DP) prepared by DP [40]; although its bimodal particle size distribution makes a comparison somewhat difficult, it is obvious that Au particles above 2 nm again yielded a considerably higher selectivity to allyl alcohol (43%, see Table 3). The low activity of the sol–gel derived catalyst could also be due to a reduction of the accessible gold surface area by either particles surrounded by titania or partially buried particles within the support framework. There may also be contributions from covering the gold by residual organic material or even by modification of the electronic properties of metal particles through their coordination to titania particles with changes of the particle size. To a first approximation a geometrical model suggested by van Hardefeld and Hartog [43] can be applied. In thermodynamic

Table 3
Catalytic results for the hydrogenation of acrolein [19][a]

Catalyst	$\bar{d}_{Au}$ (nm)	Activity (μmol g_{Au}^{-1} s^{-1})	E'_A (kJ mol^{-1})[b]	Selectivity (%)[c]				
				AyOH	PA	PrOH	HC	OP
Au/TiO_2-DP	5.3	513	58	23	58	5	5	9
Au/TiO_2-I	2.0	400	60	26	47	11	10	6
Au/TiO_2-SG	1.1	2	34	19	79	2	–	–
Au/ZrO_2-F	1.4	41	17	19	78	–	3	–
Au/ZrO_2-DP	3.8[d]	54	29	43	56	–	1	–

[a] Overall activity at $T = 513$ K, $p_{total} = 2$ MPa, H_2/acrolein = 20, $W/F^0_{Ac} = 15.3$ g h mol^{-1}.
[b] Apparent activation energy.
[c] Selectivity to: AyOH (allyl alcohol), PA (propanal), PrOH (*n*-propanol), HC (hydrocarbons: ethane, ethylene, propane, propene), OP (other products: acrylic acid, formyldihydropyran).
[d] Bimodal particle size distribution (2.1 and 7.4 nm).

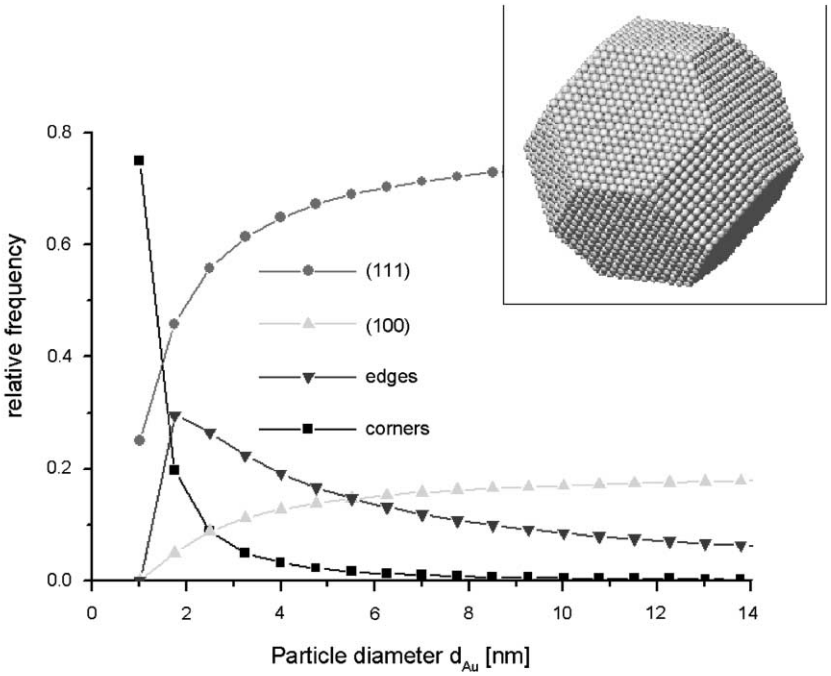

Fig. 9. Dependence of relative amounts of surface sites on particle diameter of gold particles, based on cuboctahedron model (inset) [37,43].

equilibrium, the shape of the fcc metal gold having nanometer size (at a temperature of 0 K) should be a cuboctahedron, as calculated by the so-called Wulff construction [44]. Accordingly, for increasing particle sizes the relative amount of surface atoms, especially the fraction of dense (1 1 1) planes increases as well (Fig. 9). The selectivity to the desired allyl alcohol increases with particle size, and this could imply that on the closed-packed structure of the (1 1 1) surface the C=O group is preferentially activated, whereas sites of low coordination, mostly present on small particles as corners and edges, strongly favor the activation of the C=C group according to studies on platinum single crystals [45]. If hydrogenation of the C=O group of the α,β-unsaturated aldehyde is favored by face atoms, the increased fraction of dense (1 1 1) planes of the larger gold particles should give higher formation rates of the allylic alcohol than low-coordinated atoms of smaller particles. Interestingly, this unusual catalytic behavior of gold catalysts is in line with the structure-sensitivity observed in our studies over titania supported nanosized silver particles; in the selective hydrogenation of crotonaldehyde [14], the ultradispersed 1.4 nm Ag particles gave both a lower activity and selectivity to the unsaturated alcohol than the 2.8 nm Ag particles. Investigating the same reaction Lercher and coworkers [46] observed a marked increase of selectivity towards the unsaturated alcohol with increasing fraction of Pt(1 1 1) surfaces.

Surely this geometrical effect does not influence the catalytic behavior alone. In sufficiently small particles changes of the surface coordination are linked to changes in electronic properties. Unusual electronic properties of nanosized gold should be taken into consideration in order to understand the significant changes of the hydrogenation behavior observed by down-sizing the particles, i.e. when particle sizes were <2 nm they gave one to two orders of magnitude lower catalytic activities and the olefinic double bond is hydrogenated in preference to the carbonyl group. It is likely that a marked change in the electronic character of nanosized gold particles in the 1–2 nm range may indicate a transition to the nonmetallic phase

and that the structure-sensitivity originates from a quantum-size effect. On the other hand, gold particles larger than 2–3 nm are certainly metallic in character and activate the C=O group to produce allyl alcohol with significantly higher selectivity at increased activity. Indeed, as shown by Valden et al. [17] who prepared Au/TiO_2 model catalysts by vapor deposition on single crystalline titania TiO_2 surfaces, a metal-to-nonmetal transition occurs as the gold cluster size was decreased below 300 atoms per cluster (i.e. 3.5 nm in diameter and 1.0 nm in height) giving rise to a structure-sensitivity of the oxidation of carbon monoxide.

With regard to the nature of active sites, the in-depth characterization described above showed EPR signals for F-centres in Au/ZrO_2-F and Au/TiO_2-SG. Paramagnetic F-centres, i.e. electrons trapped in oxygen vacancies have strong one-electron donating character [47]. Presumably, electron transfer takes place from the reduced support to the gold particles during the reduction procedure, and electron transfer can also take place from the support to the organic reactant during reaction. In Au/TiO_2 $Au^{\delta-}$ sites exposed at the surface of small negatively charged gold clusters were found in addition to Au^0 sites exposed at the surface of small three-dimensional particles [48]. By electron transfer due to the interaction of nanosized gold particles and F-centres or due to support reduction, gold may become enriched in valence electron density, thereby altering the interaction of the active sites with the functional group and facilitating a partial transfer of electron density to the π^* orbital of the unsaturated bond. As mentioned above, first investigations by Mössbauer spectroscopy did not confirm a negative charge on Au particles.

Regarding the activation of hydrogen, for Au/TiO_2 catalysts FT-IR studies [48] showed that H_2 dissociates on nanosized gold producing atomic hydrogen that may react with adsorbed acrolein or reduce support surface sites upon spillover. The reduction of the catalyst support, at a far lower temperature (573 K) than normally required for the occurrence of (strong) metal-support effects (>700 K), was clearly shown by EPR spectra.

Finally, comparative TEM and diffuse reflectance infrared Fourier transformation spectroscopy (DRIFTS) studies on Au/ZrO_2 and Au/TiO_2 by Baiker and coworkers [49] recently showed that in spite of similar gold particle sizes the catalytic properties in the CO oxidation are quite different. This means that apart from the gold particle size other factors seem to be crucial for catalytic activity of supported gold catalysts. The better activity of Au/TiO_2 in this oxidation reaction was explained by the number of low-coordinate gold sites being higher on TiO_2 than on ZrO_2 due to different support interactions causing different particle shapes. However, similar changes of the shape of gold particles could not be detected with TEM/HREM in the samples used in this study. In addition to the influence of particle shape, there may be an influence from defects on the gold surface. It has been known for many years that gold particles can exhibit structures differing from single crystals. The structure of these icosahedrons and decahedrons (usually called multiply twin particles) is explained by their composition of tetrahedral subunits connected by extended lattice defects [50]. Indeed Cunningham et al. [51] explained high activities of a $Au/Mg(OH)_2$ catalyst having particle sizes around 1 nm by their icosahedral crystal structure.

Another possible method to increase the intramolecular selectivity towards the allylic alcohol, not mentioned in this study, is the addition of a second metal [7,11]. Using a $Au–In/ZrO_2$ catalyst, the selectivity to allyl alcohol could be improved from 43 to 56%, even though indium itself is much less active in this reaction then silver or gold [37]. This implies that either there is an electronic modification of gold active sites due to indium or active sites on the catalyst surface responsible for propionaldehyde production are selectively poisoned by adding almost inactive indium.

3.3. Other reactions

3.3.1. Hydrogenation of butadiene

One of the first more systematic studies on the use of gold in hydrogenations was performed by Bond et al. [52] in the seventies using 1,3-butadiene as substrate. Gold was deposited by conventional impregnation on SiO_2 and Al_2O_3. Shibata et al. [53] extended these investigations to zirconia-based gold systems prepared by the oxidation of the corresponding alloys. All of these studies showed up to 100% selectivities to butene, which is otherwise achieved only on commercial palladium catalysts, but activities on Pd are markedly higher. Keeping this in mind, we

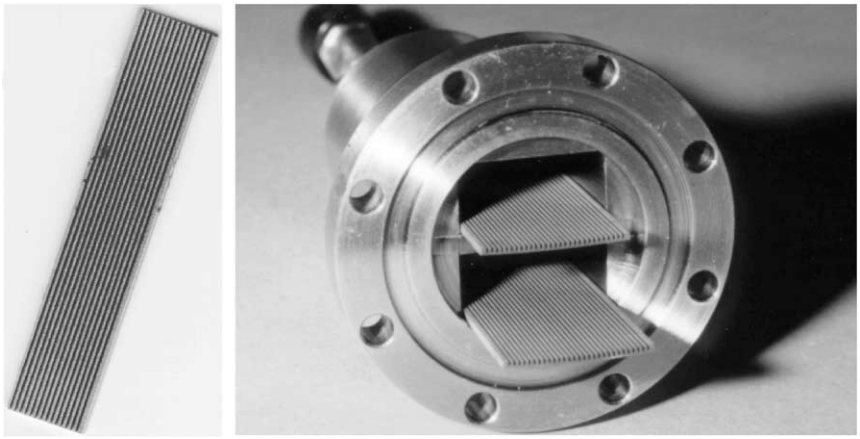

Fig. 10. Microstructured wafer, coated with alumina and gold particles, $Au/Al_2O_3/Al$ (left) and photograph of the reactor system (right).

demonstrated the practicability of microchannel reactors for regioselective hydrogenations. The inlay of this reactor type consists of microstructured Al wafers which were covered by Au/MeO_x (MeO_x: SiO_2, Al_2O_3, TiO_2, ZrO_2) layers containing very small amounts of gold (typically <0.1 wt.%). A microstructured Al wafer and the reactor system is shown in Fig. 10. The hydrogenation of 1,3-butadiene over all types of wafers gave mono hydrogenated butene selectively. The amount of 1-butene was always higher than of the isomers *trans*- and *cis*-2-butene. Furthermore, the selectivity to *trans*-butene was always higher than to *cis*-butene. The selectivity to the thermodynamically favored product *n*-butane was always below 5%. Within the temperature range (493–533 K) conversions of butadiene between 10 and 30% were achieved. As a representative example conversion and selectivity versus time on stream for a $Au/Al_2O_3/Al$ catalyst is shown in Fig. 11. At temperatures between 513 and 533 K and butadiene conversions between

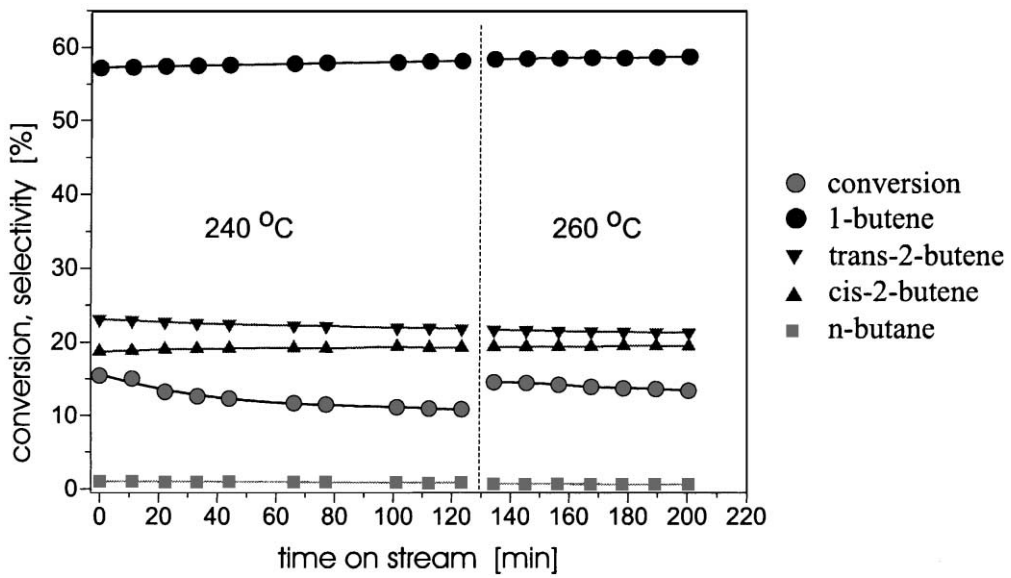

Fig. 11. Hydrogenation of 1,3-butadiene in a microchannel reactor coated with Au/Al_2O_3.

10 and 16%, the selectivities to butene were >95% with 1-butene as main product, 57% for 1-butene, 22% for *trans*-2-butene and 19% to *cis*-2-butene. Only traces of *n*-butane were observed. Fig. 11 indicates a constant deactivation of the catalysts with time [54].

The use of gold catalysts in oxidation reactions is well known, but in this study the successful use of gold catalysts for two different hydrogenation reactions has been shown. Considering the question as to why gold is active in hydrogenations at all, the adsorption and activation of both the organic molecule and hydrogen must be considered. Indeed, infrared absorption studies [55] of acrolein revealed the existence of signals related to C=O adsorption on single crystal surfaces, Au(1 1 1) as well as on polycrystalline gold films. The intensity of this signal increased with increasing coverage. Furthermore the adsorption of the organic molecule can also take place at the interface between nanosized gold particles and support or at the perimeter interface as suggested by Haruta [3] for CO oxidation. Regarding the activation of hydrogen molecule there are only very few studies dealing with the interaction of supported gold particles with hydrogen. Stobinski et al. [56] investigated the adsorption capabilities of evaporated gold in hydrogen adsorption and measured an increase in hydrogen adsorption for low gold coverages, even though this amount is still very small. This suggests a dependence of hydrogen adsorption on the increasing amount of corners and edges for decreasing gold particle sizes, i.e. a particle size dependence [2]. A chemisorption of hydrogen on supported gold is occasionally mentioned by some authors, while sometimes it has not been seen at all [2]. There exist powerful methods (for example SFG (sum frequency generation), DRIFTS and HREELS (high resolution electron energy loss spectroscopy)) to monitor the adsorption behavior [57,58] but such experiments were not yet performed with gold catalysts.

3.3.2. Low-temperature CO oxidation

A silica supported gold catalyst, prepared by organometallic chemical vapor deposition (Au/SiO_2-CVD) was used in the low-temperature oxidation of carbon monoxide. The Arrhenius plot in the temperature range of −16 to 30 °C is given in Fig. 12. For these measurements a gas hourly space velocity (GHSV) of 19.8 $l\,g_{cat}^{-1}\,h^{-1}$ was chosen. The activation energy was found to be 21.8 kJ/mol. In Fig. 12 two data points for titania supported gold catalysts estimated by Iwasawa and coworkers [59] on a gold–phosphine complex prepared catalyst and by Haruta and coworkers [60] on catalyst prepared by chemical vapor deposition are also given.

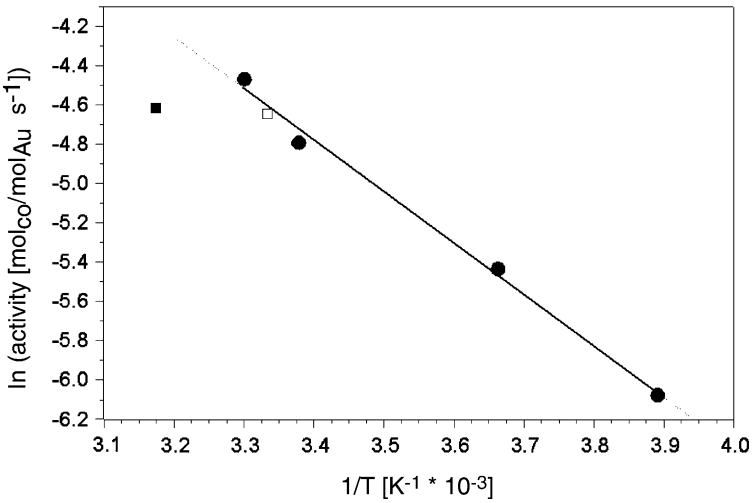

Fig. 12. Low-temperature CO oxidation using an Au/SiO_2-CVD catalyst: Arrhenius plot for the temperature range −16 to 30 °C. Open square: Au/TiO_2 (via Au–phosphine complex) [59], filled square: Au/TiO_2-CVD [60].

4. Conclusions

Nanostructural and catalytic properties have been studied in partial hydrogenation reactions, especially in the partial hydrogenation of acrolein for gold particles in the diameter range 1–6 nm deposited on titania and zirconia. Catalyst activity and selectivity to the desired allyl alcohol are increased with increasing gold particle size. This was attributed mainly to two effects, a geometrical and an electronic one. So far we conclude that adsorption of the C=O group of the α,β-unsaturated aldehyde is favored by face atoms, so that most likely the increased fraction of dense (1 1 1) planes of the larger gold particles will give higher formation rates of allyl alcohol than low-coordinated atoms of smaller-sized gold particles. From structural analysis by TEM/HREM and characterization with EPR, it was shown that the influence of small Au particles on the intramolecular selectivity of the hydrogenation of conjugated functional groups may originate from active sites comprising electron-rich gold particles formed by interaction with partially reduced support, particularly by paramagnetic F-centres entailing a strong one-electron donating character. However, this has to be confirmed or excluded by applying other characterization methods (e.g. Mössbauer spectroscopy). Apart from these considerations, the origin of the antipathetic structure-sensitivity of the hydrogenation of the C=O vs. C=C groups may be attributed to quantum-size effects which alter the electronic properties of sufficiently small gold particles. Furthermore the successful use of gold particles for the selective hydrogenation of 1,3-butadiene in a microchannel reactor could be demonstrated. Thus, the use of nanosized gold particles on oxide supports, prepared using appropriate methods, opens up new prospects for the tailoring of material properties over a wide range in the design of heterogeneous catalysts.

Acknowledgements

This work has been supported by the Federal Ministry for Science and Education under Grant 03D0028A0. PC thanks the Fonds der Chemischen Industrie and the Max-Buchner-Forschungsstiftung for financial support.

References

[1] M. Che, C.O. Bennett, Adv. Catal. 36 (1989) 55.
[2] G.C. Bond, D.T. Thompson, Catal. Rev.-Sci. Eng. 41 (1999) 319.
[3] M. Haruta, Catal. Surv. Jpn. 1 (1997) 61.
[4] R.L. Augustine, Heterogeneous Catalysts in Organic Synthesis, Dekker, New York, 1995.
[5] K. Bauer, D. Garbe, in: Ullmann's Encyclopedia of Industrial Chemistry, 6th Edition, Electronic Release, 2000.
[6] P. Claus, in: G.A. Somorjai, J.M. Thomas (Eds.), Topics in Catalysis, Special Issue "Fine Chemicals Catalysis", Part II, Vol. 5, in: D. Blackmond, W. Leitner (Eds.), Baltzer Science Publishers, 1998, p. 51.
[7] P. Gallezot, D. Richard, Catal. Rev.-Sci. Eng. 40 (1998) 8.
[8] P. Gallezot, A. Giroir-Fendler, D. Richard, Catal. Lett. 5 (1990) 169.
[9] B. Didillon, A. El-Mansour, J.P. Candy, J.P. Bournonville, J.M. Basset, in: M. Guisnet, J. Barrault, C. Bouchule, D. Duprez, G. Perot, R. Maurel, C. Montassier (Eds.), Studies on Surface Science Catalysis, Vol. 59, Elsevier, Amsterdam, 1991, p. 137.
[10] P. Claus, in: R.E. Malz (Ed.), Catalysis of Organic Reactions, Chem. Ind. Ser. 68, Marcel Dekker, New York, 1996, p. 419.
[11] V. Ponec, Appl. Catal. A 149 (1997) 27.
[12] T.B.L.W. Marinelli, V. Ponec, J. Catal. 156 (1995) 51.
[13] T.B.L.W. Marinelli, S. Naarburs, V. Ponec, J. Catal. 151 (1995) 431.
[14] P. Claus, H. Hofmeister, J. Phys. Chem. B 103 (1999) 2766.
[15] P. Claus, P. Kraak, R. Schödel, in: H.U. Blaser, A. Baiker, R. Prins (Eds.), Heterogeneous Catalysis and Fine Chemicals IV, Stud. Surf. Sci. Catal., Vol. 108, Elsevier, Amsterdam, 1997, p. 281.
[16] P. Claus, K. Schrödter, D. Hönicke, B. Lücke, in: M. Baerns, J. Weitkamp (Eds.), Selective Hydrogenation and Dehydrogenation, DGMK Report 9305, 1993, p. 239.
[17] M. Valden, X. Lai, D.W. Goodman, Science 281 (1998) 1647.
[18] G. Rupprechter, K. Hayek, H. Hofmeister, J. Catal. 173 (1998) 409.
[19] P. Claus, A. Brückner, C. Mohr, H. Hofmeister, J. Am. Chem. Soc. 122 (2000) 11430.
[20] K.-J. Berg, A. Berger, H. Hofmeister, Z. Phys. D 20 (1991) 309.
[21] M. Okumura, K. Tanacka, A. Ueda, M. Haruta, Solid State Ionics 95 (1997) 143.
[22] W. Rasband, NIH Image, Public Domain Software, US National Institute of Health. FTP: zippy.nimh.nih.gov.
[23] D.V. Mesaros, C. Dybowski, Appl. Spectrosc. 41 (1987) 610.
[24] M. Lucas, P. Claus, Chem.-Ing.-Tech. 67 (1995) 773.
[25] J.M. Montejano-Carrizales, F. Aguilera-Granja, J.L. Moran-Lopez, Nanostruct. Mater. 8 (1997) 269.
[26] J.S. Bradley, in: G. Schmid (Ed.), Cluster and Colloids—From Theory to Applications, VCH, Weinheim, 1994, p. 459.
[27] L.O. Brown, J.E. Hutchinson, J. Am. Chem. Soc. 121 (1987) 882.

[28] H. Bönnemann, W. Wittholt, J.D. Jentsch, A. Schulze Tilling, New J. Chem. 22 (1998) 713.
[29] Th. Vossmeyer, E. Delonno, J.R. Heath, Angew. Chem. 109 (1997) 1123.
[30] P.C. Ohara, J.R. Heath, W. Gelbart, Angew. Chem. 109 (1997) 1120.
[31] M. Haruta, Catal. Today 36 (1997) 153.
[32] M. Bork, R. Hoppe, A. Hofstaetter, A. Scharmann, F.E. Wagner, Z. Anorg. Allg. Chem. 622 (1996) 1721.
[33] P. Claus, S. Schimpf, R. Schödel, P. Kraak, W. Mörke, D. Hönicke, Appl. Catal. A 165 (1997) 429.
[34] R. Monot, A. Châtelein, J.-P. Borel, Phys. Lett. A 34 (1971) 57.
[35] H. Liu, L. Feng, X. Zhang, Q. Xue, J. Phys. Chem. 99 (1995) 332.
[36] S. Schimpf, J. Radnick, A. Goossens, P. Claus, in preparation.
[37] C. Mohr, P. Claus, Science in Progress, 2001, in press.
[38] J.E. Bailie, G.J. Hutchings, Chem. Commun. 21 (1999) 2151.
[39] M. Shibata, H. Kimura, T. Masumoto, J. Chem. Soc. Jpn. 6 (1990) 628.
[40] C. Mohr, H. Hofmeister, M. Lucas, P. Claus, Chem.-Ing.-Tech. 71 (1999) 869.
[41] G. Bond, Chem. Soc. Rev. 20 (1991) 441.
[42] G. Bond, Acc. Chem. Res. 26 (1993) 490.
[43] R. van Hardefeld, F. Hartog, Surf. Sci. 15 (1969) 189.
[44] C.R. Henry, Surface studies of supported model catalysts, Surf. Sci. Rep. 31 (1998) 235–325.
[45] F. Delbecq, P. Sautet, J. Catal. 164 (1996) 152.
[46] M. Englisch, A. Jentys, J.A. Lercher, J. Catal. 166 (1997) 25.
[47] P. Winiarek, J. Kijenski, J. Chem. Soc., Faraday Trans. 94 (1998) 167.
[48] F. Boccuzzi, A. Chiorino, M. Manzoli, D. Andreeva, T. Tabakova, J. Catal. 188 (1999) 176.
[49] J.-D. Grunwaldt, M. Maciejewski, O.S. Becker, P. Fabrizioli, A. Baiker, J. Catal. 186 (1999) 458.
[50] H. Hofmeister, Cryst. Res. Technol. 33 (1998) 3.
[51] E.A.H. Cunningham, W. Vogel, H. Kageyama, M. Haruta, J. Catal. 177 (1998) 1.
[52] G.C. Bond, P.A. Sermon, G. Webb, D.A. Buchanan, P.B. Wells, J. Chem. Soc., Chem. Commun. (1973) 444.
[53] M. Shibata, N. Kawata, T. Masumoto, H. Kimura, J. Chem. Soc., Chem. Commun. (1988) 154.
[54] S. Schimpf, M. Lucas, P. Claus, Selective hydrogenation of 1,3-butadiene over supported gold nanoparticles, DGMK Conference “Creating Value from Light Olefins”, October 10–12th, Hamburg, Germany, 2001, ISBN 3-931850-84-6, pp. 97–102.
[55] M. Akita, N. Osaka, K. Itoh, Surf. Sci. 405 (1997) 172.
[56] L. Stobinski, L. Zommer, R. Dus, Appl. Surf. Sci. 141 (1999) 319.
[57] G. Ertl, H. Knözinger, J. Weitkamp, Handbook of Heterogeneous Catalysis, VCH, Weinheim, 1997.
[58] G.A. Somorjai, G. Rupprechter, J. Chem. Educ. 75 (1998) 161.
[59] A.I. Kozlov, A.P. Kozlov, H. Liu, Y. Iwasawa, Appl. Catal. A 182 (1999) 9.
[60] M. Okumura, S. Nakamura, S. Tsubota, T. Nakamura, M. Azuma, M. Haruta, Catal. Lett. 51 (1998) 53.